Biophysical Chemistry 42 (1992) 133–146
Elsevier Science Publishers B.V., Amsterdam

BIOCHE 01623

Heterogeneous distributions and dispersive photodissociation rates of benzo[a]pyrene diol-epoxide enantiomer–DNA and –poly(dG-dC) · poly(dG-dC) adducts

Ryszard Jankowiak

Ames Laboratory, U.S. Department of Energy, Iowa State University, Ames, IA 50011 (USA)

(Received 8 April, 1991; accepted in revised form 26 June 1991)

Abstract

Two types of heterogeneity of adducts are illustrated and discussed utilizing non-line narrowed ($S_2 \leftarrow S_0$ laser excitation) and line-narrowed (excitation into the (0,0) origin band) fluorescence spectra at low temperatures. The first type (type A) is due to structurally distinct and/or energetically inequivalent conformers. The second one (type B) is provided by an inhomogeneous environment of DNA and polynucleotides. In light of the above, the non-exponential photodissociation kinetics of the (±)-*anti*-BPDE–DNA and -polynucleotide adducts have been reanalyzed in terms of a dispersive first order chemical reaction, where the inhomogeneous effects are explicitly included. It is demonstrated that the DNA structure shows considerable inhomogeneous broadening, and that type B heterogeneity is responsible for the dispersive photodissociation process. The latter is accounted for by a Gaussian distribution of activation energies, with the center of the distribution at ~ 600 meV and the full width at half-maximum equal to ~ 50 meV (~ 2 kT). Photolabile (±)-*anti*-BPDE–DNA and -polynucleotide adducts are identified as quasi-intercalated (site I) (+)- and (−)-*cis*-BPDE. The calculated concentrations of *cis*-BPDE adducts in DNA and polynucleotides from the kinetic data are in very good agreement with the *cis*-BPDE adduct concentrations obtained from the spectral and/or chemical analysis. The average photodissociation rate and the photodissociation quantum yield of *cis*- and *trans*-BPDE adducts are also estimated.

Keywords: Benzo[a]pyrene diol epoxide, DNA adduct; Polynucleotide adduct; Photodissociation; Conformation; Dispersion

1. Introduction

Extensive investigation, reviewed recently by Geacintov [1] and Gräslund and Jernström [2], established that the covalent binding of tumorigenic (+)-enantiomer and the non-tumorigenic (−)-enantiomer of *trans*-7,8-dihydroxy-*anti*-9,10-epoxy-7,8,9,10-tetrahydrobenzo[a] pyrene (BPDE) to double-stranded native DNA and polynucleotides, e.g. poly(dG-dC) · poly(dG-dC), gives rise to a distribution of adducts. The BPDE-adducts, which depend on the enantiomer, are characterized either as the external site II type (solvent

Correspondence to: Dr. R. Jankowiak, Ames Laboratory, U.S. Department of Energy, Iowa State University, Ames, IA 50011 (USA).

exposed binding site) or as quasi-intercalative site I type (with significant carcinogen-base stacking interaction [3–5]) adducts. It has been shown [6,7] that near ultraviolet light of relatively low fluence causes a selective photodissociation of site I adducts, while site II adducts are considerably less photolabile. The kinetics of photodissociation, without theoretical analysis, have been discussed in terms of chemical heterogeneity. For example, (+)-*anti*-BPDE–DNA adducts were characterized by a fast photodissociation rate ($k_{diss} \approx 2 \times 10^{-5}$ s^{-1}) for site I and a slow rate ($k_{diss} \approx 2.2 \times 10^{-7}$ s^{-1}) for site II type adducts [6,7].

However, over the last few years it has become clear that many physico-chemical reactions occurring in random media, e.g. glasses and proteins, follow a non-exponential kinetics [8–14]. Generally, the rate of an elementary electronic process in disordered solids can be site specific, giving rise to dispersion. For example, it has been shown that the reversible photochemical transformation of a spiropyran molecule into the merocyanine form in a polymer matrix [15] can be understood in terms of a dispersive reaction [16]. Also, studies of the annealing kinetics of light-induced metastable dangling bond defects in hydrogenated amorphous silicon provided the annealing energy distribution, which was responsible for the observed non-exponential behavior [17,18]. Further, non-photochemical hole-growth and spontaneous hole filling kinetic data of a number of molecules and/or ions in glasses and/or polymers were also successfully modeled in terms of a dispersive kinetics [8,11–13,19].

In disordered solids, there are two types of physical heterogeneity. The first type, herein referred to as type A, is due to structurally (chemically) distinct and energetically inequivalent macromolecular sites that, for example, a given adduct of BPDE–DNA (or BPDE–globin), can occupy. The recently resolved (0,0) fluorescence bands (generated with non-line narrowed $S_2 \leftarrow S_0$ laser excitation at 77 K and fluorescence quenching) with wavelengths at ~378.0 nm, 379.3 nm, 380.6 nm [20] and 382.7 nm [21] for (+)-*anti*-BPDE–DNA are a manifestation of type A heterogeneity (see Section 2). These adducts were designated as (+)-*j*, where *j* ranges from 1–4. It was also shown that the (−)-*anti*-BPDE enantiomer is chemically more heterogeneous [22,23], yielding five different adduct types, denoted as (−)-*j*, where *j* ranges from 1–5 [20]. However, our recent unpublished results indicate that (−)-5 may be a physical complex since its concentration depends on the sample age. Thus, the chemical heterogeneity of adducts from (−)-*anti*-BPDE and (+)-*anti*-BPDE may be similar although the relative distributions of (−)-*j* and (+)-*j* type adducts are dissimilar. This might be due to differences in orientation for the (+)-*j* or (−)-*j* conformers for each *j*-value. The structures of

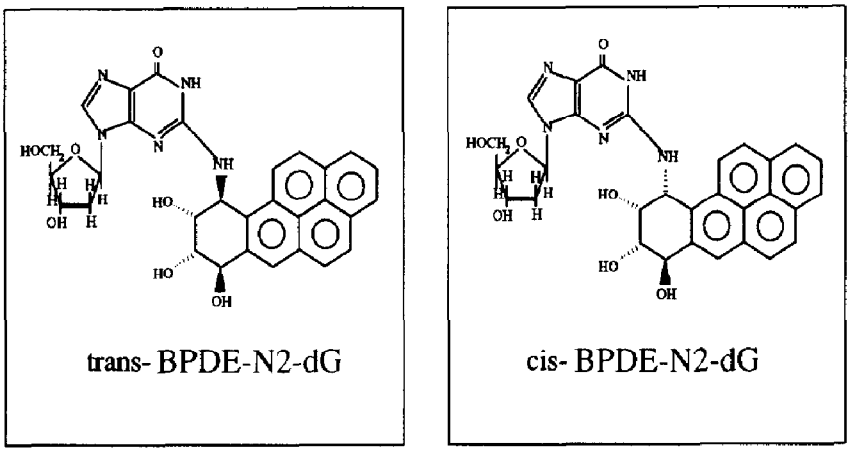

Fig. 1. Structures of *trans*-BPDE–N^2-dG and *cis*-BPDE–N^2-dG adducts, which in DNA and poly(dG-dC)·poly(dG-dC) adopt external (site II) and quasi-intercalated (site I) configuration, respectively.

trans-BPDE–N^2-dG and *cis*-BPDE–N^2-dG which in DNA and polynucleotides adopt different conformations of adducts, are shown in Fig. 1.

The vibronic absorption bands of molecules imbedded in glass, polymer, protein and nucleic acid matrices exhibit severe site inhomogeneous broadening (Γ_{inh}), which is the result of an analyte or probe molecule in a solid host adopting a very large number of energetically inequivalent sites [25]. Laser-based line narrowing spectroscopies, such as fluorescence line narrowing (FLN) [24,25] and spectral hole burning [13,26], have provided detailed information on Γ_{inh} since, in its absence, these spectroscopies are not operative. For example, hole burning has been used to show that $\Gamma_{inh} \sim 50$–$200\ cm^{-1}$ at low temperatures for chlorophylls and other cofactors in photosynthetic antenna and reaction center complexes [27]. Similarly, FLN has led to Γ_{inh}-values for macromolecular DNA and globin covalent adducts (from polycyclic aromatic hydrocarbon metabolities) which lie in the range ~ 200–$300\ cm^{-1}$ [20,21,24,25]. We will refer to the structural heterogeneity which gives rise to this type of band broadening as type B. This is a second type of heterogeneity (B) which can be viewed as having its physical origin in the inherent statistical fluctuations in the structure of the host matrix. That is, what one would view as a chemically and structurally well-defined site for the chromophore is, nevertheless, subject to heterogeneity from subtle but spectroscopically significant structural fluctuations of the host. These fluctuations lead to variations in the intermolecular interaction energies which are very small in comparison to normal chemical bond energies.

Recently, using spectral hole-burning (HB) it has been shown that daunomycin (antitumor drug) which intercalates into oligonucleotides of $d(AT)_5$ and $d(CG)_5$ exhibits inhomogeneously broadened absorption bands [28]. A factor of 60 difference in the hole burning quantum yields for two structurally distinct daunomycin-oligonucleotide complexes was observed and ascribed to the significant differences in the environment of the intercalated daunomycin.

In this paper an alternative explanation of the photodissociation results taken from Refs. [6] and [7] is presented. We will establish that type B, not type A as previously suggested [6,7], is responsible for the non-single exponential photodissociation kinetics of DNA and polynucleotide adducts from the (+)- and (−)-*anti*-BPDE. It is argued, that the dispersive kinetics arises from the fact, that the adducts sit in configurationally inequivalent environments, e.g., a particular adduct type can assume a large number of conformational substates. Therefore, we postulate that in the case of DNA-adducts, the photodissociation reactions occurring for any particular adduct type, e.g., (+)-*j*-DNA, follow dispersive kinetics, e.g., "easy" reactions will go first, since any physical quantity that depends on the interaction among neighboring sites must be subject to a distribution [8–14]. Thus, we expect that in kinetic studies of photodissociation the inhomogeneous effects must be explicitly included, since these adducts are expected to dissociate with different rates. It will be shown that the non-exponential dependence of the photodissociation process can be accounted for by a Gaussian distribution of activation energies. Finally, an attempt is made to correlate the labile BPDE-adducts with their chemical composition.

2. Experimental

2.1 Instrumentation

The fluorescence line-narrowing spectroscopy system employed in these studies has been described in detail [20,21,24]. The excitation source was a Lambda Physik FL-2002 dye laser pumped by a Lambda Physik EMG 102 MSC excimer laser. Fluorescence was detected with a Princeton Instruments IRY-1024/G/R/B intensified blue-enhanced gateable photodiode array. Gated detected was accomplished using a lambda Physik EMG-97 zero drift controller to trigger a FG-100 high-voltage gate pulse generator, which provides adjustable delay and width of the detector's temporal observation window. Samples were dissolved in 30 μL of either 5:4:1 glycerol–H_2O–EtOH or H_2O in quartz tubes, taken through several freeze–pump–thaw degassing cycles,

sealed, cooled to 4.2 K, and probed with the laser in the (0,1) and (0,0) excitation regions.

Laser-excited fluorescence spectra at 4.2 K, obtained under non-line-narrowing conditions ($S_2 \leftarrow S_0$ excitation), were measured by using an SRS Model SR280 boxcar averager (Stanford Research) equipped with two Model SR250 processor modules for channels A and B. Channel A was used to monitor the fluorescence signal, while channel B was used to monitor the pulse-to-pulse intensity jitter of the excimer pumped dye laser. All spectra reported were normalized for pulse jitter. The boxcar averager was interfaced through a SR245 computer interface module with a PC-compatible computer for data acquisition and analysis.

Kinetic experimental data were taken from Refs. [6] and [7] (see Section 5).

2.2 Materials

The DNA and polynucleotide adducts from the (+)- and (−)-*anti*-diol epoxide of benzo[a]-pyrene (for the fluorescence studies) were kindly provided by Prof. N.E. Geacintov (New York University). The preparation procedure was previously described [3–7]. The adducts (~ 1% bases modified) were diluted to a concentration (pyrenyl chromophores) of $\sim 10^{-5}$ *M*.

3. Results

3.1 Heterogeneous distributions of adducts

All broadening mechanisms for absorption bands can be categorized as either homogeneous or inhomogeneous. Homogeneous broadening is that which is the same for each and every chemically identical molecule in the ensemble. In this work, however, we are interested in the site inhomogeneous broadening which is the result of the fact that an analyte in a disordered host (DNA, proteins) can generally adopt a very large number of energetically inequivalent sites (different individual molecular micro-environments). At room temperature DNA is no longer looked upon as a static macromolecule but rather a dynamic structure in which all DNA-adduct configurations (from type B heterogeneity) are likely to be in dynamic equilibrium. However, at low temperatures most of the configurations that are thermally accessible at room temperature (depending on cooling rate) should be trapped. In this case we speak about "frozen in" disorder. Of course this also has to be true for all structurally distinct adduct types which originate from type A heterogeneity. Here it is reasonable to assume that for type A heterogeneity structurally distinct adducts (e.g., (+)-1-DNA of site II type and (+)-3-DNA of site I type), though continually fluctuating at room temperature, do not lose the strong energetic preference for the external (site II) and/or intercalated (site I) adducts types. For example, the average equilibrated energy minima for the (+)-1-DNA and (+)-3-DNA must be different, as recently demonstrated by novel energy minimization and molecular dynamic simulation studies [31].

Fig. 2A shows, as an example, the (0,0) fluorescence origin bands for (+)-*anti*-BPDE–DNA at T = 4.2 K. Spectra a and b were obtained by selective laser excitation at $\lambda_{ex} = 346$ nm and 355 nm, respectively. Spectrum a, with (0,0) band at ~ 378 nm, corresponds to the major (~ 90%), site II type adducts, (+)-*trans*-*anti*-BPDE–N^2-dG, referred to as (+)-1 [20]. Spectrum b is characteristic of site I type adducts ((+)-*cis*-*anti*-BPDE–N^2-dG) assigned to (+)-3 adduct (~ 10% [20,21]). These well-resolved (0,0) bands clearly illustrate the type A heterogenity. Spectral characteristics of site I type adducts from (±)-*anti*-BPDE in DNA and poly(dG-dC) · poly(dG-dC) at $T = 4.2$ K are summarized in Table 1. (+)-1-DNA and (+)-3-DNA (or (−)-1-DNA and (−)-3-DNA from (−)-*anti*-BPDE) can be also distinguished at room temperature [7,32] with fluorescence maxima at ~ 381 nm and ~ 383 nm, respectively.

However, the (0,0) origin bands in disordered materials, as demonstrated by [30] FLN and HB spectroscopies [25,29,33–36] are also inhomogeneously broadened. At low temperature, the fluorescence (0,0) origin bandwidth is given roughly by FWHM $\approx \Gamma_{inh} + S\omega_m$, where S is the electron-phonon coupling strength (Huang–Rhys factor) and ω_m is the mean frequency for phonons

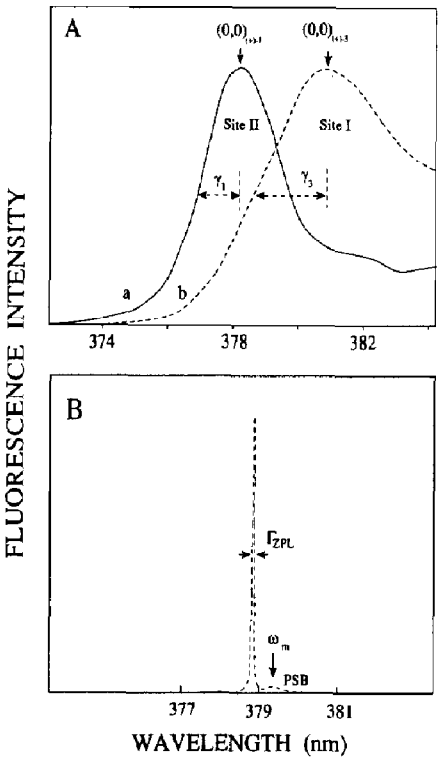

Fig. 2. (A) Inhomogeneously broadened (0,0) origin fluorescence bands of (+)-1–DNA (site II type) and (+)-3–DNA (site I type) adducts. Spectra a and b were obtained at $T = 4.2$ K under non-line-narrowing conditions for $\lambda_{ex} = 346$ nm and 355 nm, respectively. From the width of (0,0 bands, the inhomogeneous broadening (type B heterogeneity) can be estimated (see text). (B) Line-narrowed fluorescence profile of the (0,0) transition of (+)-1-BPDE–DNA adduct. The spectrum consists of an origin zero-phonon line (ZPL) coincident with $\lambda_{ex} = 378.83$ nm and, to lower energy, phonon side-band (PSB) with a mean phonon frequency $\omega_m \approx 28$ cm^{-1}. $\Gamma_{ZPL} \approx 3.5$ cm^{-1}, obtained with spectral resolution of ~ 3 cm^{-1} (see text).

which couple to the electronic transition [37]. The low-temperature widths of the (0,0) fluorescence bands (obtained under no-line narrowing conditions, e.g., $S_2 \leftarrow S_0$ excitation) of (+)-1 DNA and (+)-3-DNA are ~ 180 cm^{-1} and ~ 330 cm^{-1}, respectively. Similar values were obtained for (−)-1-DNA and (−)-3-DNA adducts from (−)-*anti*-BPDE. When broadband and/or $S_2 \leftarrow S_0$ excitation (as in Fig. 2A) is used, all adducts are excited and an inhomogeneously broadened fluorescence made up of contributions from many different sites (e.g., within the (+)-1 type adduct) is observed. If, instead, as illustrated in Fig. 2B a monochromatic source within the $(0,0)_{(+)-1}$ origin band is used, only those adducts having transitions resonant with the laser excitation within the homogeneous linewidth (Γ_{hom}) are excited and a line-narrowed fluorescence from this isochromat is observed, demonstrating type B heterogeneity. Figure 2B shows the zero-phonon line (ZPL) of (+)-1-BPDE–DNA adduct obtained for 70 ns delay time (the width of the observation window ~ 50 ns) to remove the laser light. This spectrum was obtaied at low laser light intensity ($I \sim 2$ mW/cm^2) with $\lambda_{ex} = 378.83$ nm at $T = 4.2$ K. The width of the ZPL, $\Gamma_{ZPL} = 3.5$ cm^{-1}, was slightly broader than the instrumental resolution (~ 3 cm^{-1}). The deconvolution of the instrument function would indicate the homogeneous linewidth of ~ 0.2 cm^{-1}. A zero-phonon transition is one for which no net change in the number of phonons accompanies the electronic transition. Building to higher energy on ZPL in Fig. 2B is a

Table 1

Spectral characteristic of site I type adducts from (+)- and (−)-BPDE enantiomer in DNA and poly(dG-dC)·poly(dG-dC) (≡ $(dG\text{-}dC)_2$) at $T = 4.2$ K in standard glass, $\lambda_{ex} = 355$ nm

Adduct	Fluorescence origin $\lambda_{fl}(0,0)$; nm	R [a]	$2\gamma_3(0,0)$ cm^{-1}	Quenchable by acrylamide	Conformation
(+)-3–DNA	380.6	1.15	330	no	intercalated
(−)-3–DNA	380.6	0.9	310	no	intercalated
(+)-3–$(dG\text{-}dC)_2$	~ 380.5 [b]	– [c]	~ 250 [b]	no	intercalated
(−)-3–$(dG\text{-}dC)_2$	380.6	1.0	250	no	intercalated

[a] R is the ratio of the intensity of the fluorescence origin to that of the prominent ~ 1400 cm^{-1} vibronic band, see Refs. [1] and [20].

[b] Fluorescence origin and $2\gamma_3$ (γ_3 is defined in Fig. 1A) were estimated from FLN data at $T = 4.2$ K.

[c] Not measured.

broader phonon sideband (PSB) with the average phonon frequency $\omega_m \sim 28$ cm^{-1}. Then, for example, for (±)-1-BPDE–DNA adducts, with $\omega_m = 28$ cm^{-1} (see Fig. 2B) and S ~ 0.3 (estimated by HB and FLNS), a value of $\Gamma_{inh} \sim 170$ cm^{-1} is obtained. The inhomogeneous broadening for (±)-3-DNA adducts with $\omega_m \sim 30$ cm^{-1}, and S ~ 3 (estimated by FLNS, and excitation spectra [20], data not shown) is estimated to be broader, approximately $\Gamma_{inh} \approx 240$ cm^{-1}. We believe that this type of inhomogeneity present at room temperature ("frozen-in" at low temperature) is responsible for type B heterogeneity.

Next, using FLNS, we will demonstrate that in fact it is primarily the DNA, itself, which provides this type of inhomogeneous broadening for the BPDE adducts. Figure 3 presents FLN spectra obtained with $\lambda_{ex} = 369.6$ nm (vibronic excitation) for (+)-*anti*-BPDE–DNA in standard glass (A) and in pure water only (B) ($T = 4.2$ K). This wavelength is that which was used to obtain multiplet origin structure for (+)-1-DNA adduct in the 500–800 cm^{-1} region. The spectra in Fig. 3 are virtually indistinguishable and it is apparent that the inhomogeneous broadening of BPDE–DNA in H_2O is comparable to that observed for the same adduct in glasses. This is also the case for other adducts e.g., (+)-3-DNA, though in the latter case the zero-phonon lines (ZPL) are very weak, due to much stronger electron-phonon coupling ($S \sim 3$) observed for these quasi-intercalated species [20]. Since water does not form a glass at low temperature, and a change in solvent does not significantly affect the spectra, we conclude that the disorder (inhomogeneous broadening) stems mostly from disordered DNA and not from the glass-forming solvent molecules. Hole burning phenomenon on BPDE–DNA/H_2O and BPDE–DNA/standard glass systems has been also observed. Non-exponential decay (bleaching) of the ZPL at 579 cm^{-1} in Fig. 3A has also been observed. This kind of dispersion is due to a distribution of the tunneling relaxation rates with an average tunneling parameter $\lambda_0 \sim 10.5$ and the width of its distribution $\sigma_2 \sim 0.8$ (calculated with eq. (7) from [19], for $P\sigma\omega_0/k_F = 6.13 \times 10^7$ s^{-1}), data not shown, proving that the DNA environment is in fact largely inhomogeneously broadened.

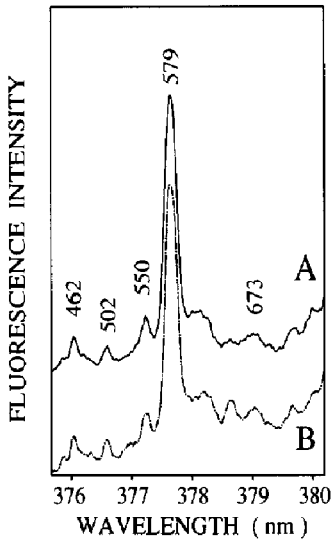

Fig. 3. Comparison of FLN spectra of (+)-*anti*-BPDE-DNA for experimental conditions which provide as the major adduct, (+)-1, in a standard glass (A) and water (B), respectively. $\lambda_{ex} = 369.6$ nm, $T = 4.2$ K. Zero-phonon lines (ZPL) are labeled with excited-state vibrational frequencies.

4. Theory of dispersive photodissociation

In our mathematical description of the photodissociation of labile BPDE-DNA and BPDE-polynucleotide adducts we use the treatment of dispersive kinetics as has been formulated by Bässler and Richert [8,10,11] and Jankowiak and Small [12,13,19].

The quantitative treatment of the problem is based on the assumption that all the photodissociation reactions are first-order which has been in fact observed by Zinger et al. [6]. Then one can write the following general equation for the BPDE–DNA adducts:

$$i(\mathit{BPDE\text{–}DNA\ adducts})\, A_S, A_L \underset{k_F}{\overset{P\sigma}{\rightleftharpoons}} (A_S + A_L)^* \xrightarrow{r_L} \mathrm{DNA} + \mathrm{BPTs} + A_S \qquad (1)$$

where BPTs (≡ benzo[a]pyrene tetraols) represent the photodissociation product, A_S and A_L stand for the density of stable and labile DNA

adducts, respectively; $P\sigma$ is the induced absorption rate, defined below; k_F is the reciprocal lifetime of the excited adducts and r_L is defined by eq. (3). A similar equation can be written for polynucleotide adducts.

Since the photodissociation follows a monomolecular decay, the concentration change of adducts as a function of time is:

$$-\frac{d}{dt}([A_S]_t + [A_L]_t) = r_S[A_S] + r_L[A_L] \quad (2)$$

where r_S and r_L are the dissociation constants for stable and labile adduct types, respectively. These decay constants are thermally activated

$$r_i(E) = \nu_0 \exp[-(E_m - E)_i/kT] \quad (3)$$

where $i = S,L$; $r_i(E)$ is the rate of the individual photodissociation reaction and $\Delta E_i = (E_m - E)_i$, denotes the spread of activation energies within mean value $E_A = \Delta E_{0i} = (E_m - E_0)_i$. Equation (1) demonstrates that the depletion of $(A_S + A_L)$ adducts and buildup of photoproducts (BPTs), under the condition of small quantum yield of photodissociation, $r_L \ll k_F$, are governed by the following rate constant:

$$R_i(E) = (P\sigma\nu_0/k_F) \cdot \exp[-(E_m - E)_i/kT] \quad (4)$$

A realistic assumption is made that the activation energy for a thermally activated reaction, is subject to a Gaussian distribution. The rationale is that the self energy of a reactant embedded in an environment with quasistatic disorder depends on a large number of internal coordinates each of which is subject to random spatial fluctuation [8–14]. This generates, as we have shown previously, a Gaussian distribution function for an experimental observable, such as the absorption profile of a chromophore in an organic glass [30] as long as the fluctuation amplitudes are small.

It has been shown that BPDE–DNA site I type adducts are of *cis*-configuration [21,37], which are about 100 times more labile than site II type (*trans*-configuration) adducts [6,7]. *Cis*-type adducts (*cis* epoxide opening) of *anti*-BPDE-dG (dG ≡ deoxyguanosine) are also less stable than their *trans*-isomer, as readily tested by the experimental data (unpublished observation). Therefore, we assume that $R_S \ll R_L$. Thus, we can simplify the picture by taking into account only labile (site I) type adducts. If the distribution of activation energies (due to inhomogeneous environment of quasi-intercalated site I type adducts) is narrow, i.e., if $|E - E_0| \ll E_0$, and if the deviation $E - E_0$ are random and independent of each other, $f(E)$ will be a Gaussian

$$f(E) = (\sigma_1\sqrt{2\pi})^{-1} \exp[-(E - E_0)^2/2\sigma_1^2] \quad (5)$$

If one accepts eqs. (1)–(5) as the relation describing the photodissociation of labile adducts, the normalized distribution function $f(R_L)$ for the dissociation rate constant is easily obtainable from eqs. (4) and (5) using the approach we developed in Ref. [12]. Then with $D(t)$ defined as

$$D(t) = \frac{([A_{L,S}]_0 - [A_{L,S}]_t)}{[A_{L,S}]_0} = D_L(t) + D_S(t) \quad (6a)$$

and $A_{L,S}(t)$ as

$$A_{L,S}(t) = \int_{-\infty}^{\infty} dR_{L,S} f(R_{L,S}) \exp[-R_{L,S}(E)t] \quad (6b)$$

$D_L(t)$ and $D_S(t)$ describe the fraction of labile (site I) and more stable (site II) adducts which dissociate following the UV irradiation for time t with an illumination photon flux P ($P = I/h\nu$). Here σ is the absorption cross section and $\phi(r_L)$ is the quantum yield of photodissociation, defined as $r_L/r_L + k_F \approx r_L/k_F \ll 1$. That $\phi(r) \ll 1$ has been observed experimentally [6,7]. Thus eqs. (6a) and (b) may be solved yielding the normalized concentration of dissociated adducts (C_L) decaying via nonconstrained first-order reactions, whose rate is given by eq. (4), and the rate controlling parameter E being subject to a Gaussian distribution function of width σ_1 (eq. 5). Assuming that mostly labile adducts dissociate (for the experimental condition, described in Fig. 1 caption) e.g., $\langle R_L \rangle \gg \langle R_S \rangle$, the experimental data may be fit to eqs. (6a) and (b). For the simulations we have found it convenient to em-

ploy a particular form for $A_{L,S}(t)$ which is equivalent to eq. (6b). Starting with

$$A_{L,S}(t) = \left(\sqrt{2\pi}\,\sigma_1\right)^{-1} \int_{-\infty}^{\infty} dE \times \exp\left[-\frac{(E_0 - E)^2}{2\sigma_1^2}\right] \exp[-R_i(E)t] \tag{7a}$$

with $R_i(E)$ given by eq. (4), it is easy to show that

$$D_L(t) = C_L\left[1 - A^{-1}\int_{-\infty}^{\infty} \exp\left\{-x^2/2\tilde{\sigma}_1^2 - t\beta \exp[-\Delta E_{0L}/kT] \exp(x)\right\} dx\right] \tag{7b}$$

where $A = \int_{-\infty}^{\infty} \exp(-x^2/2\tilde{\sigma}_1^2)\,dx$, $\tilde{\sigma}_1 = \sigma_1/kT$ and $\beta = P\sigma\nu_0/k_F$. A similar equation can be written for $D_S(t)$, since as will be shown below, that "stable" adducts also dissociate, though on a much longer time scale than the labile ones [6]; ν_0 is an attempt-to-dissociate frequency, which has been argued to be between about 2×10^{12} s^{-1} and 5×10^{13} s^{-1}, for most first-order reactions [38]. The value of a prefactor ν_0 is not very sensitive in this kind of simulation, as shown in Ref. 12, and a reasonable estimate of $\nu_0 = 8 \times 10^{12}$ s^{-1} has been utilized in this work.

Equation (7b) is solved by numerical integration for fixed values of β (*vide supra*) and for variable distribution width $\tilde{\sigma}_1$ and the average activation energy, ΔE_{0L}, for labile adducts. Equation (7b) is written in such a way that the concentration of labile adducts ($C_L \cdot 100\%$) is easily obtainable. The photodissociation data previously collected by Zinger et al. [6] and Kim [7], are reanalyzed using the above described model in Section 5. The origin of dispersion is discussed.

5. Discussion of kinetic data

In the study of adducts dissociation it is important to use illumination photon flux, P, values which are sufficiently low, as used in Refs. [6] and [7], since several studies showed that highlight intensities led to irreversible adduct photodegradation [24,39]. As shown by Zinger et al. [6] and Kim [7] the $I = 0.1$ mW/cm^2, at $\lambda_{ex} = 343 \pm 20$ nm excitation ($S_2 \leftarrow S_0$), the BPT molecules are stable for the entire period of the experiment. Interestingly, for these experimental conditions the whole distribution of adducts is initially excited (there is no correlation between S_2 and S_1 excited states) and essentially all adducts might undergo photodissociation. For completeness, Fig. 4 shows the experimental data obtained earlier [6,7], which are theoretically analyzed below. The amount of dissociation products was determined from a quantitative analysis of the increased fluorescence yield [6,7]. Curve a describes the photodissociation kinetics, as a function of time, of the (+)-*anti*-BPDE–DNA, whereas curves b and c represent the kinetics of (−)-*anti*-BPDE–DNA and (−)-*anti*-BPDE–poly(dG-dC)·poly(dG-dC), respectively. These kinetic curves when plotted on a logarithmic time scale (see data points in Figs. 5 and 7) due to the non-linearity of $D(t)$, clearly indicate a heterogeneous behavior, the nature of which will be described below.

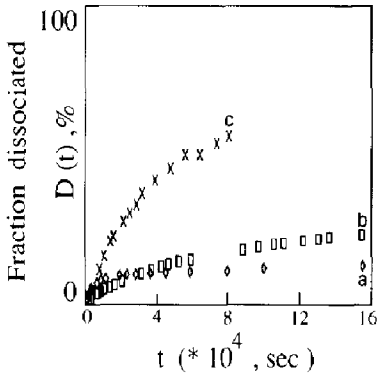

Fig. 4. Room temperature photodissociation kinetics of (+)-*anti*-BPDE–DNA [6] (◇) and (−)-*anti*-BPDE–DNA (□) and (−)-*anti*-BPDE–poly(dG-dC)·poly(dG-dC) adducts (×) [7]. $D(t)$ (the percentage of dissociated adducts) is plotted versus t ($t \equiv$ irradiation time, in s). The light intensity $I = 0.1$ mW/cm^2 at 343 ± 20 nm.

5.1 (+)-Anti-BPDE–DNA and –polynucleotide adducts

In the case of (+)-*anti*-BPDE type adducts, as shown in detail elsewhere [7,6,20] the majority of

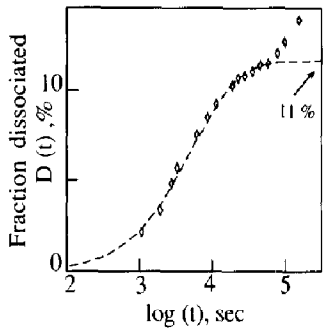

Fig. 5. Normalized theoretical fit (dashed line) obtained with Eq. 7 to the experimental photodissociation products (BPT, tetraols) growth (◇) for (+)-*anti*-BPDE–DNA plotted on a log t scale. Fit obtained with $\sigma = 1.1 \times 10^{-13}$ cm^2, $\nu_0 = 8 \times 10^{12}$ s^{-1} and $k_F = 0.67 \times 10^8$ s^{-1} [7] provides the concentration of site I type *cis*-BPDE adducts (11%) with the average activation energy for photodissociation of 600 meV.

adducts are *trans*-type of site II (external configuration). Figure 5 shows the experimental photodissociation data (diamonds) along with the theoretical fit (dashed line) which was obtained with eq. (7b) for an average activation energy $\Delta E_{0L} = 600$ meV, $\beta = 2.28 \times 10^6$ s^{-1} and a Gaussian width of the distribution of activation energies of $\tilde{\sigma}_1 = 0.83$. This provided the full-width at half maximum (FWHM $= 2\tilde{\sigma}_1\ kT\ \sqrt{2 \ln 2}$) equal to ≈ 50 meV. In addition the fitting procedure gives the concentration C_L of labile adducts of $\sim 11\%$. These data clearly demonstrate that all labile adducts have been entirely decomposed on the experimental time scale with an average dissociation rate of $\langle r_L \rangle = R_0 \exp(\tilde{\sigma}_1^2/2) = 0.56 \times 10^3$ s^{-1}, where $R_0 = \nu_0 \exp(-\Delta E_{0L}/kT)$. The observed increase of dissociation at times longer than $\sim 8 \times 10^4$ seconds indicates that at these times a slower dissociation component (characteristic for the more stable, type II adducts) emerges. Since the concentration of labile adducts, C_L, is in very good agreement with the concentration of *cis*-BPDE–DNA adducts (see Table 2) (estimated spectroscopically [6,20]), we assign the labile adducts as (+)-*cis*-*anti*-BPDE–N^2-dG.

The ΔE_{0L} and $\tilde{\sigma}_1$ values for (+)-*cis*-*anti*-BPDE–DNA along with the values for $\langle r_L \rangle$ and the corresponding average quantum yield of photodissociation, $\langle \phi_L \rangle = \langle r_L \rangle / (\langle r_L \rangle + k_F) = 0.83 \times 10^{-5}$, are given in Table 2. The value of $\langle \phi_L \rangle$ for labile adducts is approximately two orders of magnitude smaller than the quantum yield estimated previously [6]. However, due to the dispersion of photodissociation, which results from the ΔE_{0L} distribution, the quantum yield associated with, for example, the first $\xi = 5\%$ fraction of dissociated adducts $\langle \phi_L \rangle_\xi$ must be higher than $\langle \phi_L \rangle$. It can be estimated, based on the model

Table 2

Dispersive photodissociation products growth kinetic parameters for BPDE–DNA and –polynucleotides adducts at room temperature. For the kinetic analysis a value $\sigma = 1.1 \times 10^{-13}$ cm^2 and $k_F = 0.67 \times 10^8$ s^{-1} and $k_F = 1.25 \times 10^9$ s^{-1} for (+)-*anti*-BPDE- and (−)-*anti*-BPDE–adducts were used [7], respectively

Adducts	Percentage of site I type adducts etimated		Simulation data				
	Spectroscopically	Chemically	Concentration [a] of site I type (*cis*-BPDE) adducts, $C_L \times 100\%$	Average activation energy (meV)	$\tilde{\sigma}_1$	Average dissociation rate $\langle r_L \rangle$ (s^{-1})	Average quantum yield for dissociation $\langle \phi_L \rangle$
(+)-*Anti*-BPDE–DNA	14 [6,7] ~ 10 [b]	–	11	600	0.83	0.56×10^3	0.83×10^{-5}
(−)-*Anti*-BPDE–DNA	~ 30 [b]	–	29	591	0.83	0.79×10^3	0.63×10^{-6}
(+)-*Anti*-BPDE–(dG-dC)$_2$	10 [40]	14 [41]	~ 13	598	0.80	0.55×10^3	0.81×10^{-5}
(−)-*Anti*-BPDE–(dG-dC)$_2$	73–75 [7,40] ~ 70 [b]	71 [41]	74	580	0.80	1.1×10^3	0.2×10^{-6}

[a] $C_s = 100 - C_L$ (%) describes the concentration of site II type adducts at room temperature.
[b] This work.

we developed in Ref. [19], studying the dispersive kinetics of hole growth in disordered systems, that in fact $\langle \phi_L \rangle_{\xi=5\%}$, for (+)-*anti*-BPDE–DNA, is a factor of ~ 60 higher, indicating a moderate dispersion of photodissociation process. Nearly identical values of the average activation energy and dissociation rate were obtained for (+)-*anti*-BPDE adducts in polynucleotide poly(dG-dC)·poly(dG-dC) (data not shown), as illustrated in Table 2. Interestingly, the estimated concentration (C_L) of site I type (+)-*cis*-BPDE adducts is nearly the same in DNA and poly(dG-dC)·poly(dG-dC) duplex. This may indicate that in fact (+)-3 adducts of (+)-BPDE enantiomer prefer the G-C DNA sequence. It is noteworthy that $C_L \approx 13\%$ for (+)-*anti*-BPDE-poly(dG-dC)·poly(dG-dC) is in nearly perfect agreement with recent chemical analysis in which Geacintov et al. [41] estimated the concentration of (+)-*cis*-BPDE adducts as $C_L \approx 14\%$. These data prove that the observed nonlinearity of the experimental data in Fig. 5 stems from type B disorder, which is reflected by the inhomogeneous broadening of (+)-(3) type (*cis*-BPDE) adducts. It is the local disorder (due to arrangement of certain atoms, groups of atoms and bonds [42]) which makes the adducts energetically different.

5.2 Distribution in energy

There are several approaches one may take to derive the activation energy distribution directly from experimental decay and/or growth kinetic curves. If, for example, a decay $A_{L,S}(t)$ given by eq. (6b) possesses a unique distribution $f(R_{L,S})$, the latter can be derived by the inverse Laplace transform of the analytic continuation of $A_{L,S}(t)$. Alternatively, to derive $f(R_{L,S})$ one can apply various analysis methods: e.g., nonlinear least squares fitting [43] or the method of moments [44]. Another approach has been recently developed by Jackson et al. [45]. These authors described an iterative method for systematically obtaining distributions of annealing and/or creation energies, tunneling distances, and trap depths for specific defect populations from electron-spin resonance transients. For example, this method was used to obtain, based on a molecular annealing model, the distribution of activation energies of metastable dangling bond defects in light-soaked undoped hydrogenated amorphous silicon (a-Si:H) [18]. Below, adopting this approach [1,5,18] we will show that the activation energy distribution $P(E_A)$ can be determined, for (+)-*anti*-BPDE–DNA labile adducts from the adduct photodissociation decay curve, defined as $y(t) = 1 - D(t) = [A_L]_t/[A_L]_0$. It has been shown that in good approximation

$$\frac{d}{dE_A} y(t) \approx -P(E_A,0) \tag{8}$$

where the activation energy is defined as:

$$E_A = kT \ln(\beta t) \tag{9}$$

By taking the derivative of $y(t)$ with respect to $kT \ln(\beta t)$, the underlying distribution of activation energies, E_A, can be derived. This can be done if the dynamic range of experimental data is sufficiently large, as in the case of (+)-*anti*-BPDE-DNA, see Fig. 5. The derived original activation energy distribution $P(E_A, 0)$ at time $t = 0$, for the above discussed (+)-*anti*-BPDE–DNA is presented in Fig. 6. Using this approach $P(E_A)$ can be easily reconstructed step by step from any experimental data where the distribution of kinetic parameters is involved. However, because of the approximation introduced above

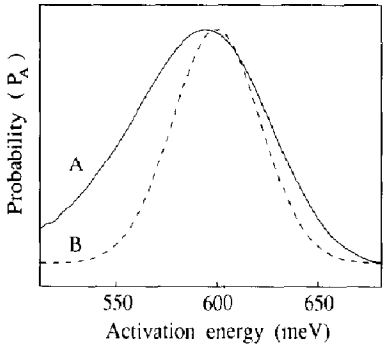

Fig. 6. Normalized probability distribution of activation energies (curve A) versus energy of the investigated labile (+)-*anti*-BPDE–DNA (*cis*-type) adducts as derived from the dashed curve in Fig. 5 using eq. (8). For comparison (curve B) shows the normal distribution of activation energies obtained with the simulated parameters of $\Delta E_{0L} = 600$ meV and $\tilde{\sigma}_L = 0.83$, used to fit the data in Fig. 5.

(eq. 8), some discrepancies between the calculated curve for $P(E_A)$ (curve A, in Fig. 6) and the Gaussian $P(E_A)$ assumed *a priori* (curve B) in our simulation, were anticipated. Note that the correct position of the peak in the distribution (within the resolution of ~5 meV) is recovered with some broadening especially on the low energy side. This is not surprising since curve A in Fig. 6 was obtained from an analysis where all of the time dependence, contained in the exponential factor in eq. (6b) has been neglected. This is equivalent to the approximation sometimes used in the analysis of the dispersive kinetics (for very large dispersion) [12], which when adopted to the time dependent photodissociation can be written (instead of eq. 6b), as:

$$A_L(t) \approx \int_{E_{min}(t)}^{\infty} f(E_A)\, dE_A \qquad (10)$$

In eq. (10) $f(E_A)$ is the distribution of the activation energies, and $E_{min}(t)$ is the lower cut-off energy. This simplified procedure, as shown in Fig. 6 and discussed in Refs. [10] and [12], provides an accurate approximation only for very large dispersion compared to the spread of event times at fixed rate. Thus, the numerical equivalence of eqs. (6b) and (10) increases for increasing variance of the rate-controlling parameters responsible for dispersive kinetics.

5.3 (−)-anti-BPDE–DNA and polynucleotide adducts

In contrast to (+)-*anti*-BPDE–DNA adducts, the (−)-*anti*-BPDE–DNA adducts show, on similar time scale, much larger percentage of photodissociated products. The experimental kinetics data of photodissociation of (−)-*anti*-BPDE in DNA (from Ref. [6]) and poly(dG-dC)·poly(dG-dC) (from Ref. [7]) are depicted in Fig. 7A. The simulation curves, which are indicated as dashed lines, were obtained (for $\beta = 1.22 \times 10^5\ s^{-1}$) with eq. (7b), provided: $\langle E_A \rangle = 580$ meV, $\tilde{\sigma}_1 = 0.80$ and $C_L = 74\%$ for (−)-*anti*-BPDE–polynucleotide adducts (curve a) and $\langle E_A \rangle = 591$ meV, $\tilde{\sigma}_1 = 0.83$ and $C_L = 29\%$ for –DNA adducts (curve B), respectively. This figure shows that, the dispersive kinetic model is not only in very good agreement with the experimental results, but also provides the relative concentration of labile adducts in these two systems (see the numbers over the arrows) on the right vertical scale in Fig. 7A). The estimated concentration of labile adducts is ~74% and ~29% for polynucleotide and –DNA samples, respectively. As in the case of (+)-*anti*-BPDE those numbers are in very good agreement with the concentration of site I type adducts in these two systems, estimated spectroscopically, see Table 2. Remarkably, $C_L \approx$ 74% for (−)-*anti*-BPDE-poly(dG-dC)·poly(dG-dC) obtained from simulation analysis is not only in very good agreement with the concentration of site I type adduct (*cis*-BPDE) obtained spectroscopically [7,40] but also with recent chemical analysis [41]. Therefore, as above (see Section 5.1), we correlate these adducts with *cis* diol epoxide opening. Interestingly, the average activation energy for (−)-BPDE adduct in two differ-

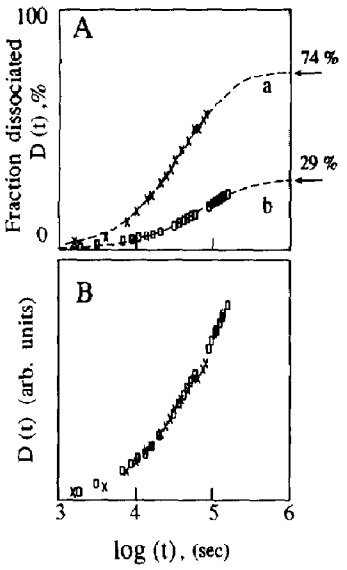

Fig. 7. (A) Theoretical fits (- - - - - -) to the dissociation products (BPTs) growth $D(t)$ (%), plotted versus log of irradiation time for (−)-*anti*-BPDE-poly(dG-dC)·poly(dG-C) (×) and (−)-*anti*-BPDE–DNA (□), respectively. The fits were obtained with σ and ν_0 given in Fig. 5 caption and with $k_F = 1.25 \times 10^9\ s^{-1}$ [7]. The calculated concentration of *cis*-BPDE adducts is ~74% (a) and ~29% (b) for the polynucleotide and DNA, respectively. (B) Normalized experimental data from curves a and b (in Fig. 7A) taking into account the estimated relative adduct concentration.

ent hosts are also nearly identical, with slightly narrower $\tilde{\sigma}_1$ value for –poly(dG-dC)·poly(dG-dC). In native DNA $\tilde{\sigma}_1$ is expected to be larger, because there is more than one type of base-triplet involving dG adducts. Interestingly, $\tilde{\sigma}_1 = 0.83$ is similar to the width of the conformational barrier distribution (trapped at $T = 4.2$ K) in a chromoprotein, where $\tilde{\sigma} \approx 1$ has been observed [14].

The major difference for (–)-BPDE adducts refers to the concentration (C_L) of site I type adducts, which is ~2.6 times smaller in DNA than in $(dG\text{-}dC)_2$. With this in mind in Fig. 7B, we present the data from Fig. 7A in a normalized form where the concentrations of –DNA and –polynucleotide adducts from Fig. 7A were normalized. This comparison clearly demonstrates that the kinetics of photodissociation in DNA and a double strand of poly(dG-dC)·poly(dG-dC), though very different in appearance in Fig. 4, is in fact identical when the relative concentration (C_L) of labile adducts is taken into account. This is not surprising, since, as we have shown in this work, in both cases the labile adducts had the same chemical composition.

This is also in agreement with our recent low-temperature spectroscopic findings for adducts in random sequence DNA and an alternating duplex of poly(dG-dC)·poly(dG-dC), which showed indeed very similar conformational features [21,32]. The photodissociation activation energies for (–)-*anti*-BPDE-adducts range from ~520 to ~660 meV, with the center of the distribution at ~590 meV and the FWHM of the Gaussian distribution approximately equal to 50 meV (~2 kT). The average rate and quantum yield for photodissociation of (–)-*anti*-BPDE–DNA and polynucleotide adducts are also listed in Table 2. Comparing (+)- and (–)-*anti*-BPDE–DNA and –polynucleotides, in contrast to Refs. [6] and [7] only a small difference between the average relaxation rates, $\langle r_L \rangle$, is observed. For example, $\langle r_L \rangle$ for (–)-*anti*-BPDE–DNA adducts is about 1.4 times larger than for their (+)-enantiomer. However, the $\langle \phi_L \rangle$ value for (+)-type DNA adducts is ~13 times larger than for (–)-BPDE–DNA adducts. Likewise, a similar difference in $\langle \phi_L \rangle$ (a factor of ~10) between (+)-*anti*-BPDE- and (–)-*anti*-BPDE–poly(dG-dC)·poly(dG-dC) is observed. This can be ascribed to the differences of their average relaxation rates and the reciprocal lifetimes (k_F) of the excited adducts, as can be seen from the definition of $\langle \phi_L \rangle$ given in Section 5.1. The difference in $\langle \phi_L \rangle$ between the pair of (+)- and (–)-enantiomer adducts for the (+)-3 and (–)-3 category of adducts has been anticipated in light of recent spectroscopic data [20,21] which showed that site I type adducts of these two enantiomers (though intercalated) may be situated differently with respect to the DNA, e.g. they possess different R ratio, see Table 1. The small orientational differences may be an inherent aspect of the mirror image nature of the (+)- and (–)-*anti*–BPDE adducts, and perhaps could explain why the DNA adopts higher concentration (~3 times) of (–)-BPDE–*cis*-type adducts. On the other hand, similarities in activation energy and $\langle r_L \rangle$ values for all studied systems are not surprising, since in all cases mostly labile (site I) (+)- and (–)-*cis*-BPDE adducts dissociated.

The dynamic range of the photodissociation data is not sufficient to describe the more stabe (+)-1 type adducts. Nevertheless, based on the slower dissociation component (circles in Fig. 5A), for the more stable adducts, assuming similar $\tilde{\sigma}_1$ value as for labile ones, the average activation energy for these (+)-1 type adducts (site II, *trans*-N^2-dG) can be roughly estimated. Its average value of ~750 meV, is about 150 meV higher than for *cis*-BPDE intercalated adducts. This means that the average relaxation rate and the average quantum yield for photodissociation of *trans*-BPDE–N^2-dG (site II) adducts compared to *cis*-type adducts is approximately 2–3 orders of magnitude smaller.

It is worth noting that recently for a number of proteins, e.g., a tryptophan residues in different proteins [46] and chlorophyll *a* in photosystem II reaction center preparation [47], a continuous distribution of fluorescence lifetimes were observed. Therefore, a question that arises is whether or not the distribution of the fluorescence lifetime (τ) of site I type adducts (if present) would significantly affect the values of $\langle E_A \rangle$ and $\langle r_L \rangle$. The answer is no, since as discussed in

Ref. [10] this type of additional dispersion is negligible compared to a fluctuation of the exponential factor in eq. (4), namely $(E_m\text{-}E)/kT$.

In conclusion, we believe that the non-exponential photodissociation can be explained by postulating, in analogy to a number of proteins [14,46,47], that DNA-adducts of each particular adduct type (from type A heterogeneity), exist in many different conformational substates and that the adducts in different substates possess different activation energies for the photodissociation reaction described by eq. (1). Since disordered systems break ergodicity [48], the equilibrium distributions in configuration space are of little use. Therefore, the activation energy (barrier height) which dominate the photodissociation process depends, as demonstrated, on the observation time scale. Although we believe that the room-temperature dispersion must be dynamic in nature, where the dynamics of the system determines the interconversion between conformation substates, a static origin in which a unique activation energy is associated with every element of a distribution of conformational substates cannot be entirely excluded.

Acknowledgments

The Ames Laboratory is operated for the U.S. Department of Energy by Iowa State University under contract no. W-7405-Eng-82. This work was supported by the Office of Health and Environmental Research, Office of Energy Research. The author thanks J.M. Hayes and G.J. Small for a critical reading of the manuscript and N.E. Geacintov for providing preprints of Refs. [31], [40] and [41] prior to publication.

References

1 N.E. Geacintov, Mechanisms of reaction of polycyclic aromatic epoxide derivatives with nucleic acids, In: Polycyclic aromatic hydrocarbon carcinogenesis: Structure–activity relationships, Vol. 2, eds. S.K. Yang and B.D. Silverman, (CRC Press, Boca Raton, FL, 1988) pp. 181–206.
2 A. Gräslund and B. Jernström, Q. Rev. Biophys. 22 (1989) 1.
3 N.E. Geacintov and A.G. Gagliano, Carcinogenesis 3 (1982) 247.
4 R.G. Harvey and N.E. Geacintov, Acc. Chem. Res. 21 (1988) 66.
5 V. Kolubayev, H.C. Brenner and N.E. Geacintov, Biochemistry 26 (1987) 2638.
6 D. Zinger, N.E. Geacintov and R.G. Harvey, Biophys. Chem., 27 (1987) 131.
7 S.K. Kim, Ph.D. Dissertation, New York University, NY, 1990.
8 R. Jankowiak, R. Richert and H. Bässler, J. Phys. Chem. 89 (1985) 4574.
9 W. Siebrand and T.A. Wildman, Int. Rev. Phys. Chem. 5 (1986) 251.
10 R. Richert, J. Chem. Phys. 86 (1987) 1743.
11 A. Elschner, R. Richert and H. Bässler, Chem. Phys. Lett. 127 (1986) 105.
12 R. Jankowiak, L. Shu, M.J. Kenney and G.J. Small, J. Lumin. 36 (1987) 293.
13 R. Jankowiak and G.J. Small, Science 237 (1987) 618.
14 W. Köhler, J. Friedrich and H. Scheer, Phys. Rev. A 37 (1988) 660.
15 G. Smets, Adv. Polym. Sci., 50 (1983) 17.
16 R. Richert and H. Bässler, Chem. Phys. Lett. 116 (1985) 149.
17 W.B. Jackson and M. Stutzman, Appl. Phys. Lett. 49, (1986) 957.
18 M. Stutzman, W.B. Jackson and C.C. Tsai, Phys. Rev. B 34 (1986) 63.
19 M.J. Kenney, R. Jankowiak and G.J. Small, Chem. Phys. 146 (1990) 47.
20 R. Jankowiak, P. Lu, G.J. Small and N.E. Geacintov, Chem. Res. Toxicol. 3 (1990) 39.
21 P. Lu, H. Jeong, R. Jankowiak, G.J. Small, S.K. Kim, M. Cosman and N.E. Geacintov, Chem. Res. Toxicol. 4 (1991) 58.
22 P. Brooks and M.R. Osborne, Carcinogenesis 3 (1982) 1223.
23 S.C. Cheng, B.D. Hilton, J.M. Roman and A. Dipple, Chem. Res. Toxicol. 2 (1989) 334.
24 R. Jankowiak and G.J. Small, Anal. Chem. 61 (1989) 1023A.
25 R. Jankowiak and G.J. Small, Chem. Res. Toxicol. 4 (1991) 256.
26 R. Jankowiak, S.R. Cooper, D. Zamzow, G.J. Small, G. Doskocil and A.M. Jeffrey, Chem. Res. Toxicol. 1 (1988) 60.
27 S.G. Johnson, I.-J. Lee and G.J. Small, in: Chlorophylls, ed. H. Scheer (and references therein).
28 G. Flöser and D. Haarer, Chem. Phys. Lett. 147 (1988) 288.
29 G. Marsch, R. Jankowiak, G.J. Small, N.C. Hughes and D.H. Phillips, Chem. Res. Toxicol. (submitted 1991).
30 R. Jankowiak, K.-D. Rockwitz and H. Bässler, J. Phys. Chem. 87 (1983) 552.
31 S.B. Sing, B.E. Hingerty, U.Ch. Singh, J.P. Greenberg, N.E. Geacintov and S. Broyde, Cancer Res. 51 (1991)

3482.
32 H. Jeong, R. Jankowiak, P. Lu, G. Marsch, G.J. Small, M. Cosman, S.K. Kim and N.E. Geacintov (in preparation).
33 J.K. Gillie, J.M. Hayes, G.J. Small and J.H. Golbeck, J. Phys. Chem. 91 (1987) 5524.
34 I. Renge, K. Mauring and R. Avarma, Biochim. Biophys. Acta 766 (1984) 501.
35 R. Jankowiak, D. Tang, G.J. Small and M. Seibert, J. Phys. Chem. 93 (1989) 1649.
36 R.J. Personov, Characteristics of noncovalent and covalent interactions of (+) and (−) anti-benzo[a]pyrene diol-epoxide stereoisomers of different biological activities with DNA, in: Spectroscopy and excitation dynamics of condensed molecular systems, eds. V.M. Agranovich and R.M. Hochstrasser (North Holland, Amsterdam, 1983) Vol. 4 pp. 555–616.
37 N.E. Geacintov, M. Cosman, V. Ibanez, S.S. Birke and C.E. Swenberg, Site selection spectroscopy of complex molecules in solutions and its applications, in: Molecular basis of specificity in nucleic acid–drug interactions, eds. B. Pullman and J. Jortner (Kluwer Academic, Dordrecht, 1990).
38 T.L. Cottrell, in: Strengths of chemical bonds (Butterworths, London, 1954) p. 53..
39 T.C. Boles and M.E. Hogan, Proc. Natl. Acad. Sci. U.S.A. 81 (1984) 5623.
40 C.J. Roche, A.M. Jeffrey, B. Mao, A. Alfano, S.K. Kim, V. Ibanez and N.E. Geacintov, Chem. Res. Toxicol. 4 (1991) 311.
41 N.E. Geacintov, M. Cosman B. Mao, A. Alfano, V. Ibanzes and R.G. Harvey (1991) preprint.
42 M. Techera, L.L. Doemen and E.W. Prohofsky, Phys. Rev A 42 (1990) 1008.
43 A.E. McKinnon, A.G. Szabo and D.R. Miller, J. Phys. Chem. 81 (1977) 1564.
44 I. Isenberg, J. Chem. Phys. 59 (1973) 5696.
45 W.B. Jackson, M. Stutzman and C.C. Tsai, Phys. Rev. B 34 (1986) 54.
46 J.R. Alcala, E. Gratton and F.G. Prendergast, Biophys. J. 51 (1987) 597.
47 Govindjee, M. van de Ven, C. Preston, M. Seibert and E. Gratton, Biochim. Biophys. Acta 1015 (1990) 173.
48 R.G. Palmer, Adv. Phys., 31 (1982) 669.